

# Cyclodextrin-Modified CeO<sub>2</sub> Nanoparticles as a Multifunctional Nanozyme for Combinational Therapy of Psoriasis

This article was published in the following Dove Press journal:  
*International Journal of Nanomedicine*

Lingyun Wu<sup>1,2,\*</sup>  
Guoyan Liu<sup>2,\*</sup>  
Wenyu Wang<sup>1</sup>  
Ruobing Liu<sup>1</sup>  
Lingyan Liao<sup>1</sup>  
Ni Cheng<sup>1</sup>  
Wentong Li<sup>3</sup>  
Weifen Zhang<sup>1</sup>  
Dejun Ding<sup>1</sup>

<sup>1</sup>College of Pharmacy, Weifang Medical University, Weifang, Shandong 261053, People's Republic of China; <sup>2</sup>Department of Dermatology, Affiliated Hospital of Weifang Medical University, Weifang 261031, People's Republic of China; <sup>3</sup>Department of Pathology, Weifang Medical University, Weifang, Shandong 261053, People's Republic of China

\*These authors contributed equally to this work

**Purpose:** Reactive oxygen species (ROS)-induced oxidative stress plays a key role in the pathogenesis and progression of psoriasis by causing inflammation. Antioxidative strategies eradicating ROS may serve as effective and easy treatment options for psoriasis, while nanozymes with intrinsic antioxidant enzyme-like activity have not been explored for psoriasis treatment. The aim of this study is to fabricate  $\beta$ -cyclodextrins ( $\beta$ -CDs)-modified ceria nanoparticles ( $\beta$ -CDs/CeO<sub>2</sub> NPs) with drug-loaded and multimimic-enzyme activities for combinational psoriasis therapy.

**Methods:** The  $\beta$ -CDs/CeO<sub>2</sub> NPs were synthesized by a hydrothermal method using unmodified  $\beta$ -CDs as a protecting agent. The structure, size and morphology were analyzed by dynamic light scattering, transmission electron microscopy (TEM), X-ray photoelectron spectroscopy (XPS) and Fourier transform infrared (FTIR) spectroscopy. Considering the superoxide dismutase (SOD)- and catalase-mimetic activities, the in vitro antioxidant activity of the  $\beta$ -CDs/CeO<sub>2</sub> NPs was investigated. After dithranol (DIT) was loaded, the drug-loading capacity and release profile were determined by UV-visible light spectrophotometer and high-performance liquid chromatography. The anti-psoriatic efficacy was studied in the imiquimod (IMQ)-induced mouse model on the basis of morphological evaluation, psoriasis area and severity index calculation (PASI), and inflammatory cytokine expression.

**Results:** The average particle size of the blank  $\beta$ -CDs/CeO<sub>2</sub> NPs was 60.89±0.32 nm with a polydispersity index (PDI) of 0.12, whereas that of the DIT-loaded NPs was 79.38±1.06 nm with a PDI of 0.27. TEM results showed the as-prepared NPs formed a uniform quasi-spherical shape with low polydispersity. XPS indicates synthesized NPs have a mixed Ce<sup>3+</sup>/Ce<sup>4+</sup> valence state. FTIR spectroscopy confirmed the presence of  $\beta$ -CDs and DIT in the NPs. Inhibition of superoxide anion rate by NPs could be reached to 79.4% in the presence of 200  $\mu$ g/mL, and elimination of H<sub>2</sub>O<sub>2</sub> efficiency reached about 50% in the presence of 40  $\mu$ g/mL, demonstrating excellent superoxide dismutase- and catalase-mimicking activities, thereby providing remarkable cryoprotection against ROS-mediated damage. Furthermore,  $\beta$ -CDs on the surface endowed the NPs with drug-loading function via host-guest interactions. The entrapment efficiency and drug loading of DIT are 94.7% and 3.48%, respectively. The in vitro drug release curves revealed a suitable release capability of DIT@ $\beta$ -CDs/CeO<sub>2</sub> NPs under physiological conditions. In IMQ-induced psoriatic model, the DIT@ $\beta$ -CDs/CeO<sub>2</sub> NPs exhibited excellent therapeutic effect.

**Conclusion:** This study may pave the way for the application of nanozyme  $\beta$ -CDs/CeO<sub>2</sub> NPs as a powerful tool for psoriasis therapy.

**Keywords:** ceria nanoparticles, reactive oxygen species, mimic-enzyme, dithranol, anti-psoriatic, drug delivery

Correspondence: Weifen Zhang; Dejun Ding  
College of Pharmacy, Weifang Medical University, 7166# Baotong West Street, Weifang, Shandong 261053, People's Republic of China  
Tel/Fax +(86)-0536-8462051  
Email zhangwf@wfmuc.edu.cn; dejunding@wfmuc.edu.cn

## Introduction

Psoriasis is a chronic inflammatory skin disease clinically featured by erythematous plaques covered with silvery scales.<sup>1,2</sup> Psoriasis would cause high morbidity due to pain, itching, functional and cosmetic impairments, and even high mortality due to depression and suicidal contemplations. The prevalence of psoriasis is currently estimated to be as high as 2–3% worldwide, becoming a serious global problem.<sup>3–5</sup> Moreover, it is also associated with many comorbidities such as psoriasis arthritis,<sup>6</sup> metabolic syndrome<sup>7</sup> and cardiovascular disease,<sup>8</sup> which brings huge health and economic burden to patients. Although various immune abnormalities have been proposed to be involved in the pathogenesis of psoriasis,<sup>9</sup> oxidative stress is also believed to play a pivotal role in the pathophysiological mechanism. Increased production of ROS would induce a vast number of biological responses to the initiation of psoriasis pathogenesis.<sup>10–12</sup> ROS including superoxide anion ( $O_2^{\bullet-}$ ),  $\bullet OH$  free radicals and nonradical molecules such as  $H_2O_2$  would induce oxidative damage, such as lipid peroxidation, DNA modification, and secretion of inflammatory cytokines in psoriatic derma.<sup>11,12</sup> Oxidative damage markers including malondialdehyde, lipid hydroperoxides, thiobarbituric acid reactive substances, protein carbonyl, and nitric oxide have been detected in patients with psoriasis.<sup>11,13</sup> Therefore, antioxidative strategies eradicating ROS may serve as effective and easy treatment options for psoriasis.<sup>14</sup> Antioxidants, such as epigallocatechin-3-gallate,<sup>15</sup> glabridin,<sup>16</sup> proanthocyanidins,<sup>17</sup> polyandric acid<sup>18</sup> and other natural compounds<sup>19,20</sup> with beneficial effects on cutaneous psoriasis have been reported.

Recently, nanomaterials with enzyme-like activity named nanozymes,<sup>21,22</sup> have been exploited as potential therapeutics in various diseases, including Parkinson's disease,<sup>23</sup> Alzheimer's disease,<sup>24</sup> cancer,<sup>25–27</sup> ischemic stroke,<sup>28,29</sup> and ischemia reperfusion injury,<sup>30</sup> through mainly eliminating ROS levels in cells. For instance,  $Mn_3O_4$  nanozymes have been used as a promising therapeutic agent for treating inflammation because of their excellent ROS scavenging activity.<sup>23</sup> Ceria nanoparticles (CeNPs) exhibit tremendous potential as effective antioxidant enzymes, such as peroxidase, oxidase, catalase, and SOD.<sup>31,32</sup> These high-performance ROS reduction capacities originate from the dual oxidation states ( $Ce^{3+}/Ce^{4+}$ ) on the surface of these particles in which  $Ce^{3+}$  is responsible for eliminating  $O_2^{\bullet-}$  and  $\bullet OH$ , while  $Ce^{4+}$  eradicating  $H_2O_2$ .<sup>32</sup> CeNPs have been applied to treat various ROS-associated diseases, including ischemic stroke,<sup>33</sup> rheumatoid arthritis,<sup>34</sup> autoimmune degenerative disease.<sup>35</sup> Nowadays,

nanodermatology is an emerging field that uses nanotechnology to facilitate the diagnosis and treatment of skin disease.<sup>36,37</sup> However, most of them are inorganic nanomaterials lack of multi-functional and have not been explored for psoriasis treatment.

To fill this research gap, we designed a multifunctional drug delivery system based on CeNPs capped with  $\beta$ -CDs for psoriasis treatment (Scheme 1).  $\beta$ -CDs/CeO<sub>2</sub> NPs exhibit high mimetic enzymatic activity to eliminate intracellular ROS, rendering them ideal antioxidants for the treatment of oxidative stress-induced damage in psoriasis. Moreover, the introduction of  $\beta$ -CDs, a family of cyclic oligosaccharides,<sup>38,39</sup> on the surface of CeNPs increases their water solubility, biocompatibility, and antioxidant property. Furthermore, the porous nanostructures with unique hydrophobic  $\beta$ -CDs cavity could be used as a promising drug carrier for hydrophobic molecules by supra-molecular inclusion.<sup>40,41</sup> In the present study, we investigated the drug-loading ability and anti-psoriasis activity of  $\beta$ -CDs/CeO<sub>2</sub> NPs on IMQ-induced psoriasis-like mouse model by using DIT as the lipophilic model drug.

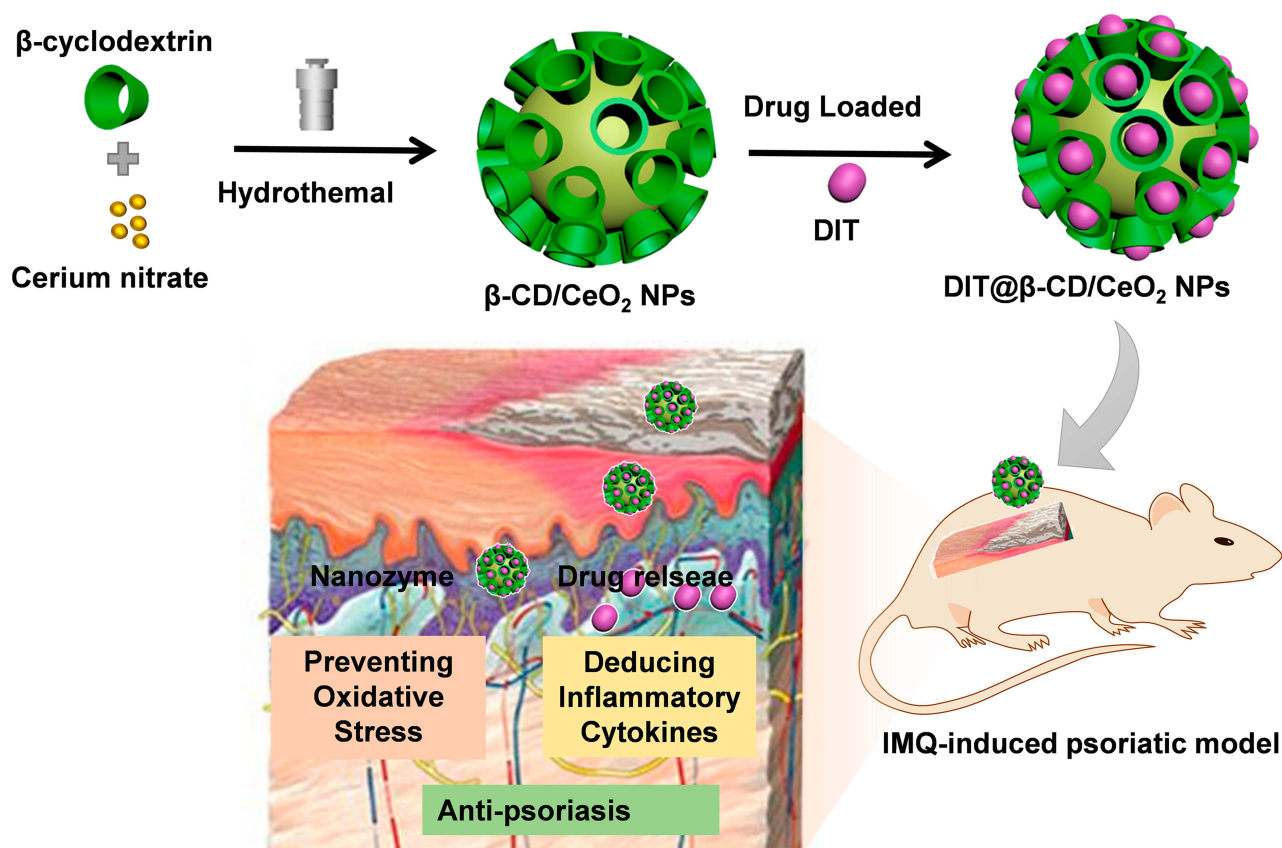
## Materials and Methods

### Materials

DIT was obtained from Yuanye Biotechnology Co. Ltd. (Shanghai, China).  $\beta$ -CDs were purchased from Kelong Chemical Reagent Factory (Chengdu, China). Cerium nitrate was obtained from Bodi Chemical Company Co. Ltd. (Tianjin, China). Carbopol 940 was supplied by Tianliyuan Biotechnology Co. Ltd. (Qingdao, China). IMQ was purchased from Mingxin Pharmaceutical Co. Ltd. as a topical cream (5% imiquimod; Sichuan, China). Halometasone cream (0.05%) was purchased from Huabang Pharmaceutical Co. Ltd. (Chongqing, China). Paraformaldehyde (4%) was obtained from Biosharp Biological Technology (Anhui, China). Methanol was attained from Tedia Compang (high purity, US). Sodium sulfide was purchased from Hengxing Chemical Reagent Company Co. Ltd. (Chengdu, China).

### Animals

Male BALB/c mice (6–8 weeks old) were purchased from Qingdao Darenfucheng Animal Husbandry Co. Ltd. (Qingdao, China) and housed under specific pathogen-free conditions by the Experimental Animal Center, Weifang Medical University (Weifang, China). All of the animal experiments performed in strict accordance with the recommendations in the Guide for the Care and Use of Laboratory Animals published by the Weifang Medical University. The



**Scheme 1** Schematic interpretation of the design of β-cyclodextrin capped ceria nanoparticles as a nanozyme loaded with dithranol for the combinational therapy of psoriasis.

protocol was approved by the Committee on the Ethics of Animal Experiments of Weifang Medical University (Permit Number: 2019SDL096). The treatment of experimental animals followed the 3Rs principles. All experiments were abided by the ethical principles of experimental animal welfare, and every effort was made to minimize suffering.

## Cells Line and Cells Culture

The HaCaT human keratinocyte cells line was obtained from Procell Life Science & Technology Co. Ltd. (Wuhan, China) and cultured in RPMI 1640 medium (Gibco, NY, USA) supplemented with 15% fetal bovine serum (Beijing, China), 100 U/mL penicillin, and 100 mg/mL streptomycin. The cells were maintained at 37°C with 5% CO<sub>2</sub> in a humidified incubator. The growth medium was replaced every 2–3 days.

## Preparation of DIT-Loaded β-CDs/CeO<sub>2</sub> NPs

The synthesis of β-CDs capped CeO<sub>2</sub> NPs were performed according to previous literature.<sup>42</sup> Cerium nitrate solid particles were added to 30 mL of distilled water, and ultrasonic

cleaner was used to dissolve it completely. β-CDs solid was added and stirred with a magnetic stirrer for 10 min. The colorless liquid became a white mixture. Then, NaOH solid was added to the mixed solution slowly and stirred for another 15 min. The white mixture changes to a reddish brown liquid. The prepared mixture liquid was placed at 125°C for 6 h using a hydrothermal method, cooled to room temperature, and then left at room temperature for 12 h. The solution of blank NPs was slowly dropped into the dissolved DIT in different concentrations, and the optimal particle size was selected as the dose concentration.

## Characterization of DIT@ β-CDs/CeO<sub>2</sub> NPs

The particle size distribution and polydispersity index (PDI) of the blank NPs and drug-loaded NPs were determined in triplicate at 25°C using a Zeta Sizer Nano ZS90 (Malvern Instruments, Malvern, UK). The morphologies of the blank NPs and drug-loaded NPs were observed by TEM (Tecnai 20, FEI, USA). Measurements were performed in triplicate for each sample. A standard curve was obtained for DIT using a UV-visible light

spectrophotometer at 289 nm, and the drug loading (DL) and entrapment efficiency (EE) were measured. The DL (%) and EE (%) were calculated as follows:

$$\text{Drug loading (\%)} = \frac{\text{Actual amount of drug encapsulated in NPs}}{\text{Amount of NPs}} \times 100\%$$

$$\text{Entrapment efficiency (\%)} = \frac{\text{Actual amount of drug encapsulated in NPs}}{\text{Initial amount of drug used}} \times 100\%$$

The chemical structure of the prepared NPs was characterized using Fourier transform infrared spectrometry (FT-IR; VERTEX 70; Bruker, Bremen, Germany). The spectra of the samples of  $\beta$ -CDs, cerium nitrate, DIT,  $\beta$ -CDs/CeO<sub>2</sub> NPs, and DIT@ $\beta$ -CDs/CeO<sub>2</sub> NPs were obtained separately. X-ray photoelectron spectroscopy (Ultima IV; Rigaku Corporation, Japan) was used to investigate the microstructure of the  $\beta$ -CDs/CeO<sub>2</sub> NPs.

### In vitro Release of DIT@ $\beta$ -CDs/CeO<sub>2</sub> NPs

In vitro drug release study of DIT@ $\beta$ -CDs/CeO<sub>2</sub> NPs and free DIT solution was conducted by the dialysis bag method (molecular weight cut-off 12,000 Da).<sup>43</sup> Release media consisted of acetate buffer pH 3.3 and Milli-Q water in the proportion 50:50 containing 0.5% (v/v) Tween-80. Free DIT solution (2 mg in 2 mL 1% DMSO) and DIT@  $\beta$ -CDs/CeO<sub>2</sub> NPs (corresponding DIT amount was 2 mg, 2 mL) were added separately into the dialysis bags and then immersed in 10 mL of release medium at 37°C with a shaking speed of 100 rpm. At predetermined time points, 500  $\mu$ L of sample was collected, and fresh media replacement was done after sampling. The quantity of DIT was measured using the Shimadzu Prominence high-performance liquid chromatography system and C 18 analytic column (Luna C18(2) 25 cm $\times$ 4.6 cm, 5 mm, Phenomenex Inc, Torrance, CA). The mobile phase is a mixture of methanol and water (80:20, volume/volume ratio). The UV absorbance was measured at a wavelength of 289 nm, with a flow rate of 1.0 mL/min and a 25- $\mu$ L injection volume. Standard curve has been measured by applying HPLC. All samples are prepared in triplicate.

### SOD- and Catalase-Mimetic Activity Assay

The SOD-mimetic activity of the  $\beta$ -CDs/CeO<sub>2</sub> NPs was investigated through its O<sub>2</sub><sup>•-</sup> scavenging activity with the Total Superoxide Dismutase Assay Kit with nitro-blue tetrazolium (NBT, Biotech, China) as described in the previous literature.<sup>44</sup> In brief, 20  $\mu$ L of the  $\beta$ -CDs/CeO<sub>2</sub> NPs dispersion at different concentrations (0, 5, 10, 20, 40, 80, 160, and 200  $\mu$ g/mL) was incubated with assay reagent containing xanthine, xanthine oxidase, and NBT into a 96-well plate at 37°C for 30 min. The absorbance at 560 nm was then recorded using a Multiskan GO microplate reader (Thermo Scientific, USA), and the O<sub>2</sub><sup>•-</sup> inhibition rate was calculated in accordance with the manufacturer's formula.

Catalase-mimicking activity was measured with the catalase assay kit (Biotech, China). In brief, a H<sub>2</sub>O<sub>2</sub> standard curve was drawn by different concentrations (0, 0.0025, 0.005, 0.01, 0.015, and 0.02  $\mu$ M).<sup>45</sup> Then, we prepared a blank control and a sample solution (0, 5, 10, 20, 40, 80, 160, 200  $\mu$ g/mL) and reacted at 25°C for 5 min. A stop solution and color-developing solution were added, and then the solution was incubated at 25°C for 15 min. Then, the absorbance at 520 nm was recorded using a Multiskan GO microplate reader (Thermo Scientific, USA), and the catalase activity was calculated in accordance with the manufacturer's formula.

### 3-(4,5-Dimethylthiazolyl)-2,5-Diphenyltetrazolium Bromide (MTT) Assay

The potential cytotoxicity of  $\beta$ -CDs/CeO<sub>2</sub> NPs was investigated in MTT assay as we reported earlier.<sup>46</sup> The HaCaT human keratinocyte cells line was selected to analyze cell viability in MTT assay (Sigma, MO, USA). HaCaT human keratinocyte cells were seeded into 96-well plates at a concentration of 1 $\times$ 10<sup>4</sup> cells/well and then incubated at 37°C and 5% CO<sub>2</sub> for 24 h to ensure proper stability and adherence. Then, the culture medium was removed. The cells were incubated with fresh medium containing 100  $\mu$ g/mL  $\beta$ -CDs/CeO<sub>2</sub> NPs for 24 h before 20  $\mu$ M H<sub>2</sub>O<sub>2</sub> was added. After 24 h of cell culture, 10  $\mu$ L of MTT (5 mg/mL) was added into each well. Incubation was continued for 4 h, and then 100  $\mu$ L of DMSO was appended to each well to dissolve MTT crystals. The reactions were monitored using an iMark microplate reader (Bio-rad, CA, USA) at a wavelength of 490 nm. The experiment was repeated three times.

## Cellular ROS-Scavenging Activity

The role of nanocarriers in scavenging ROS was investigated using 2',7'-dichlorodihydrofluorescein diacetate.<sup>46</sup> The HaCaT human keratinocyte cells line was selected and seeded into 12-well plates at a concentration of  $4 \times 10^4$  cells/well. Cells were incubated at 37°C and 5% CO<sub>2</sub> for 24 h to ensure proper stability and adherence, and then the culture medium was removed. Then,  $\beta$ -CDs/CeO<sub>2</sub> NPs (100  $\mu$ g/mL) were added in the different wells, except in the positive control wells. After 24 h, serum-free medium (1 mL) with 20  $\mu$ M H<sub>2</sub>O<sub>2</sub> was added to each well, except the blank hole. After 6 h, the wells were added with 2',7'-dichlorodihydrofluorescein diacetate (ROS fluorescence probe), incubated for another 20 min, and then observed under fluorescence microscopy.

## Experiments on BALB/c Mice

### IMQ-Induced Plaque-Like Mouse Model of Psoriasis

IMQ-induced psoriasis-like mouse model was established as previously described.<sup>47</sup> Male BALB/c mice (6–8 weeks old) were fed a standard diet and provided with free water at room temperature. IMQ is a TLR7/8 ligand and a potent immune activator. A psoriasis model was established as previously described with slight modifications. In specific, IMQ was administered locally to induce and aggravate psoriasis lesions. After 1 week of adaptive feeding, the back shaving area was 2 cm $\times$ 3 cm. IMQ cream (5%) was applied to the shaved area at the back of the mouse every 24 h for 8 consecutive days (50 mg per mouse), the skin lesions were observed by taking photos every day, and the PASI score was obtained. Animals were randomly grouped as follows: Group 1 (normal mice), Group 2 (mice with IMQ treatment only and induced psoriasis), Group 3 (mice treated with 1 mg of DIT-loaded  $\beta$ -CDs/CeO<sub>2</sub> NPs), Group 4 (mice treated with 0.04 mg of DIT), Group 5 (normal mice treated with 1 mg of DIT-loaded  $\beta$ -CDs/CeO<sub>2</sub> NPs), and Group 6 (halometasone cream as positive control, 0.1 mg per mouse daily). The second group served as a negative control group, and the sixth group served as a positive control group.

### Evaluation of PASI

To assess the severity of lesions at the back of the psoriatic mice, we followed the clinical criteria of PASI and established an objective scoring system to evaluate the degree of inflammation on the back lesions of the

mice.<sup>47</sup> Erythema, scaling, and thickening were scored independently by two people on a scale of 0 to 4 (0, none; 1, slight; 2, moderate; 3, marked; and 4, very marked). The scoring was performed every day for 8 days.

### Histopathology of Mouse Back Skin Lesion

The induced dorsal skin lesions were collected at the end of the 8th day, soaked, and then fixed with 4% paraformaldehyde. The fixed samples were dehydrated and embedded in paraffin. Then, 4  $\mu$ m microtome sections of the skin were deparaffinized, rehydrated, and stained with hematoxylin and eosin (H&E) as described previously.<sup>47</sup> Histopathological sections were observed under a microscope (BN-DC-RGB500, Nanjing, China).

### Weight Ratio of Spleen to Body (Spleen/Body Wt%)

The spleen is the largest immune organ in the human immune system. The weight of the spleen is a sensitive indicator of the body's immune status. The increase in spleen/body mass fraction may reflect the increase in the number of immune-related cells in the spleen, which is associated with diseases related to inflammation and immune activation.<sup>43</sup> The body weight of the mice was recorded, and then the spleen of the mice was dissected at the end of the eighth day. Finally, the spleen/body wt % was obtained.

### Immunofluorescence Staining

Tumor necrosis factor (TNF)- $\alpha$  plays a key role in the pathogenesis of psoriasis. The levels of TNF- $\alpha$  were detected by immunofluorescence staining of lesions to explore the therapeutic mechanism of DIT-loaded  $\beta$ -CDs/CeO<sub>2</sub> NPs in the psoriatic mice. Immunofluorescence staining was performed by a routine staining method.<sup>20</sup> Rabbit polyclonal antibody to TNF- $\alpha$  (1:150, Abcam) was used as the primary antibody, and anti-rabbit antibody (1:250, Proteintech) was used as the secondary antibody.

### Statistical Analysis

Data were analyzed with Statistical Package for the Social Sciences version 16.0 software (SPSS Inc., Chicago, IL, USA). The experiments were carried out in triplicates, and values are expressed as mean  $\pm$  standard deviation (SD). Student's *t*-test was conducted to determine significance. Statistical significance was considered at a probability level of  $p < 0.05$ .

## Results and Discussion

### Synthesis and Characterization of $\beta$ -CDs-Capped CeO<sub>2</sub> NPs

Generally, CeNPs are synthesized in the organic phase and require further surface modification with hydrophilic ligands for biomedical applications.<sup>48</sup> In the present study, the  $\beta$ -CDs/CeO<sub>2</sub> NPs were synthesized by a hydrothermal method using unmodified  $\beta$ -CDs as a protecting agent.<sup>42</sup> Several recent studies used  $\beta$ -CDs as a metal NP stabilizer and size-control agent due to its strong hydroxyl binding to the surface of metal NPs.<sup>49–51</sup> The lipophilic drug (DIT) was loaded in the hydrophobic inner cavity of  $\beta$ -CDs via host–guest interactions.<sup>40,41</sup> The drug EE of DIT was 94.7%, indicating that DIT was highly exhibited in these NPs and the corresponding DL reached to 3.48%.

The particle size distribution and PDI of the blank and drug-loaded NPs were determined using dynamic light scattering. The average particle size of the blank  $\beta$ -CDs/CeO<sub>2</sub> NPs was 60.89±0.32 nm with a PDI of 0.12 (Figure 1A), whereas that of the DIT-loaded NPs was 79.38±1.06 nm with a PDI of 0.27 (Figure 1B). TEM results showed that the as-prepared NPs formed a uniform quasi-spherical shape with low polydispersity, and the diameter was consistent with the above particle size measurement results and without obviously visible aggregation among the particles (Figure 1C and D). The enzyme-mimicking activities of nano-cerium are due to the presence of mixed oxidation states.<sup>32,48</sup> Thus, XPS was performed to determine the mixed oxidation states. In the XPS spectrum (Figure 1E), the peaks at 883.5, 900.1, and 917.5 eV corresponded to Ce<sup>4+</sup>, whereas the peaks at 889.5, 903.1, and 908.1 eV were related to Ce<sup>3+</sup>. The results indicate that the synthesized NPs have a mixed-valence state (Ce<sup>3+</sup>/Ce<sup>4+</sup>).<sup>21,31,32</sup>

The bio-composite complex formation of the synthesized particles was further attested through Fourier transform infrared spectroscopy by analyzing the characteristic peaks involved. As shown in Figure 1F, the presence of  $\beta$ -CDs was confirmed on the nanoceria particle surface. The main peak at 3419 cm<sup>-1</sup> was associated with OH stretching, and the peak at 3448 cm<sup>-1</sup> in the  $\beta$ -CDs/CeO<sub>2</sub> NPs involved the interaction between nanoceria and OH.<sup>49</sup> Bands appeared at 1368 cm<sup>-1</sup> (bending mode of CH<sub>2</sub>), 1157 cm<sup>-1</sup> (asymmetric C-O-C stretching), and 1029 cm<sup>-1</sup> (C-O stretching) in free  $\beta$ -CD and in the  $\beta$ -CDs/CeO<sub>2</sub> NPs. Compared with free  $\beta$ -CDs, the decreased relative intensity of the bands at 937 cm<sup>-1</sup> (skeletal vibration of 1.4 link bond), 755 cm<sup>-1</sup> (ring vibration), and 707 cm<sup>-1</sup> (pyranose ring vibration) in

the  $\beta$ -CDs/CeO<sub>2</sub> NPs were attributed to the “fixed” nature of the  $\beta$ -CDs on the nanoceria surface that prevented the pyranose ring and skeletal vibration.<sup>50</sup> Because of the existence of  $\beta$ -CDs, the NPs can be dispersed efficiently into the water solutions even at a high concentration of 15 mg·mL<sup>-1</sup>, the sediments are observed clearly in the samples without of  $\beta$ -CDs (Figure 2A). This result implies that the introduction of  $\beta$ -CDs on the surface of CeNPs increased their water solubility. After DIT was loaded, the characteristic peaks of DIT at 1614 and 1446 cm<sup>-1</sup> (aromatic ring skeletal vibrations) and 1073, 929, and 747 cm<sup>-1</sup> (C-H in- and out-plane bending) were found in the DIT@ $\beta$ -CDs/CeO<sub>2</sub> NPs. This finding confirmed the presence of DIT in the NPs.

The drug release behavior of DIT@  $\beta$ -CDs/CeO<sub>2</sub> NPs in vitro was studied and release profiles are shown in Figure 2B. The figure clearly indicates almost 85.3±1.1% DIT were released from free DIT solution in 8 h, whereas DIT release from the NPs was comparatively slow, it showed 73.3 ± 1.6% in 60 h. It is evident that DIT@  $\beta$ -CDs/CeO<sub>2</sub> NPs exhibited an obvious sustained-release profile with no evident burst effects. The pronged-release of DIT from NPs can be explained on the basis that the drug is encapsulated into the hydrophobic  $\beta$ -CDs cavity by supra-molecular inclusion.

### SOD- and Catalase-Mimicking Activity of $\beta$ -CDs/CeO<sub>2</sub> NPs

As major antioxidant enzymes, SOD and catalase can protect organisms involved in the neutralization of ROS.<sup>52</sup> The SOD- and catalase-mimetic activities of the  $\beta$ -CDs/CeO<sub>2</sub> NPs were investigated. SOD, an important antioxidant enzyme in living organisms, can catalyze the deuteration of O<sub>2</sub>•<sup>-</sup>s to H<sub>2</sub>O<sub>2</sub> and oxygen. SOD-mimicking activity was studied by the classical NBT chromogenic method. In brief, the O<sub>2</sub>•<sup>-</sup> was produced by the xanthine and xanthine oxidase reaction systems, which further reduced to be detectable blue formazan at 560 nm.<sup>44</sup> In the presence of  $\beta$ -CDs/CeO<sub>2</sub> NPs, the absorbance of formazan considerably decreased due to its SOD-mimicking activity. As shown in Figure 2C, the  $\beta$ -CDs/CeO<sub>2</sub> NPs possessed catalase-mimicking activity in a dose-dependent manner. The O<sub>2</sub>•<sup>-</sup> inhibition rate reached to 79.4% in the presence of 200  $\mu$ g/mL dispersion.

Considering that H<sub>2</sub>O<sub>2</sub> is a common form of ROS,<sup>52</sup> we studied the H<sub>2</sub>O<sub>2</sub>-scavenging activity of the  $\beta$ -CDs/CeO<sub>2</sub> NPs. Such H<sub>2</sub>O<sub>2</sub> scavenging activity can be attributed to the catalase-mimicking activity of the nanoparticles.<sup>45</sup> When H<sub>2</sub>O<sub>2</sub> is sufficient, catalase can catalyze H<sub>2</sub>O<sub>2</sub> to produce

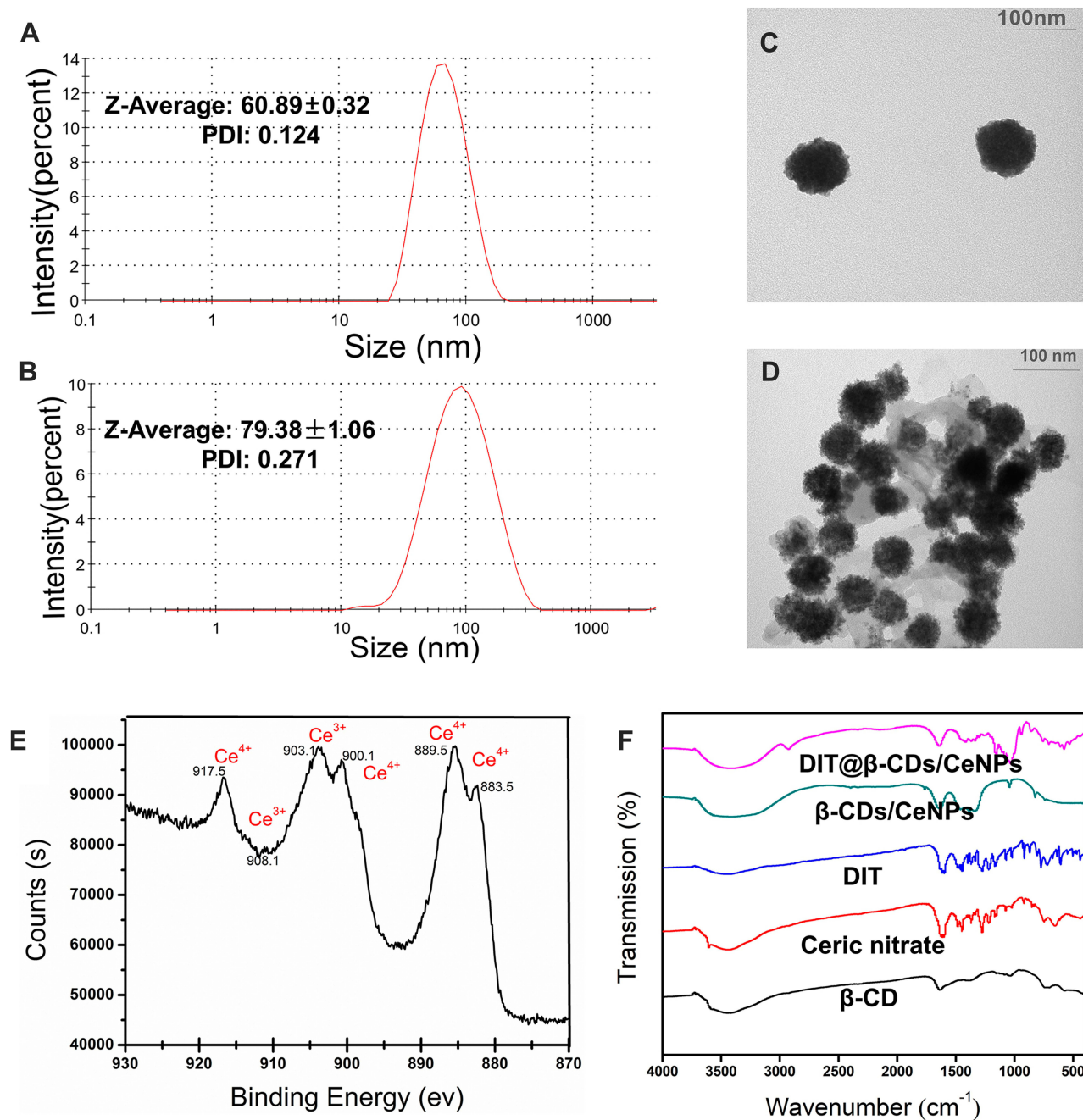


**Figure 1** Hydrodynamic diameters of  $\beta$ -CDs/CeO<sub>2</sub>NPs (A) and DIT@ $\beta$ -CDs/CeO<sub>2</sub> NPs (B) measured by DLS; TEM (scale bar = 100 nm) images of  $\beta$ -CDs/CeO<sub>2</sub>NPs (C) and DIT@ $\beta$ -CDs/CeO<sub>2</sub> NPs (D) dispersed in water; (E) XPS analysis of  $\beta$ -CDs/CeO<sub>2</sub> NPs for Ce<sup>3+</sup> and Ce<sup>4+</sup> showing the binding energy levels; (F) Fourier transform infrared spectra of  $\beta$ -CDs, ceric nitrate, DIT,  $\beta$ -CDs/CeO<sub>2</sub> NPs and DIT@ $\beta$ -CDs/CeO<sub>2</sub> NPs.

water and oxygen. The remaining H<sub>2</sub>O<sub>2</sub> coupled with a substrate and catalyzed by peroxidase to generate a red product, (N-(4-antipyryl)-3-chloro-5-sulfonate-*p*-benzoquinone monoimine), would be detected at 520 nm.<sup>45</sup> As expected, the concentration of H<sub>2</sub>O<sub>2</sub> decreased with increasing concentration of  $\beta$ -CDs/CeO<sub>2</sub> NPs (0–200  $\mu$ g/mL), as shown in Figure 2D. The H<sub>2</sub>O<sub>2</sub> eliminated efficiency reached about 50% in the presence of 40  $\mu$ g/mL  $\beta$ -CDs/CeO<sub>2</sub> NPs.

All of the above results clearly demonstrated that the  $\beta$ -CDs/CeO<sub>2</sub> NPs could play as SOD and catalase mimics. CeNPs possess SOD- and catalase-mimicking activities due to the mixed valence states of Ce<sup>3+</sup> and Ce<sup>4+</sup>.<sup>21,31,32</sup>

### Intracellular ROS Scavenging Detection

Considering their potential SOD- and catalase-mimetic activities, we investigated the in vitro antioxidant activity

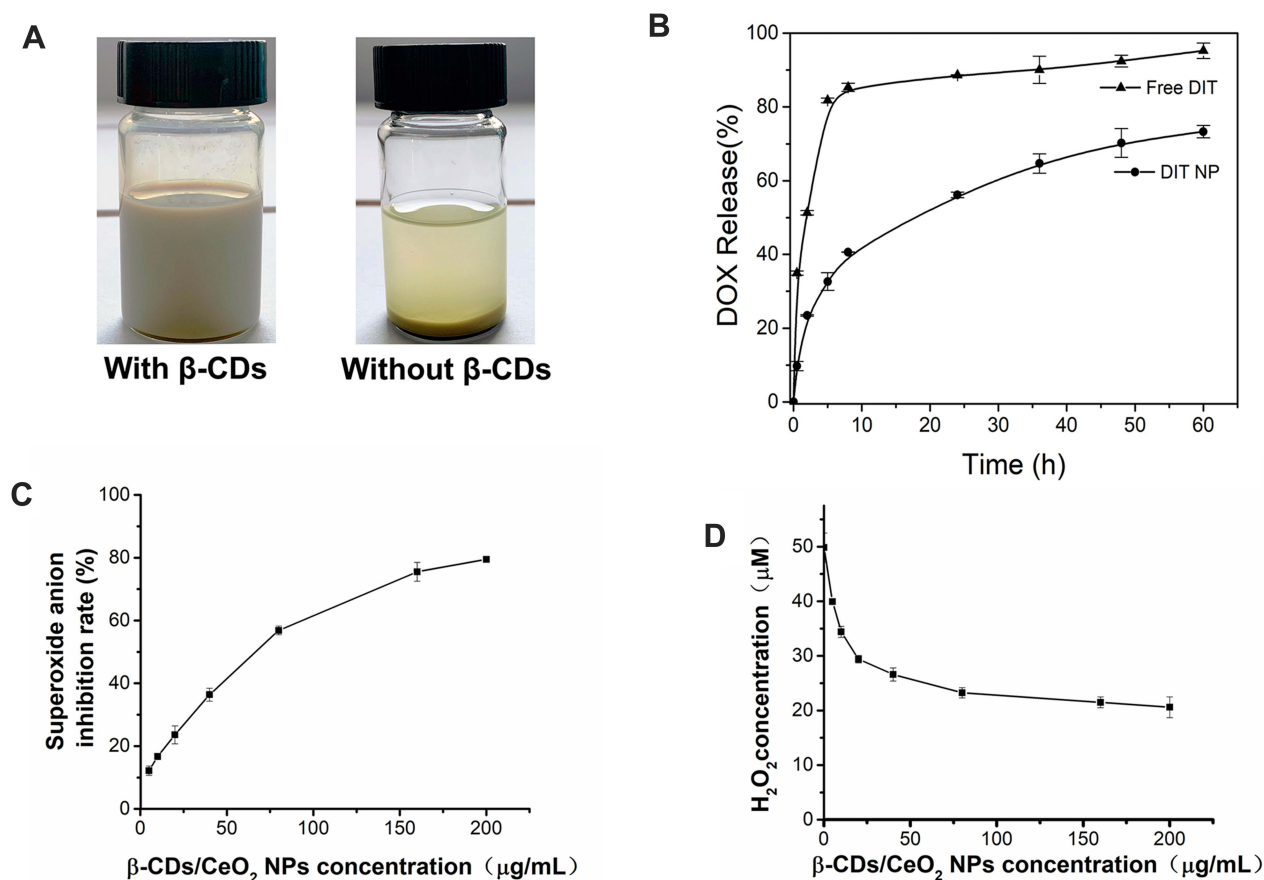


**Figure 2** (A) Photographs of 15 mg/mL CeO<sub>2</sub> with or without β-CDs; (B) The in vitro release profile of dithranol from β-CDs/CeO<sub>2</sub> NPs; suspension of superoxide anions (C) and scavenging activities of H<sub>2</sub>O<sub>2</sub> (D) by β-CDs/CeO<sub>2</sub> NPs.

of the β-CDs/CeO<sub>2</sub> NPs for protecting cells from oxidative damage using the HaCaT cells line as a model. First, the possible toxicity of the β-CDs/CeO<sub>2</sub> NPs was evaluated through MTT assay. The viability of the cells treated with β-CDs/CeO<sub>2</sub> NPs (0–250 μg/mL) in the experimental conditions was not obviously altered compared with the control groups (Figure 3A). Then, we examined the effectiveness of the β-CDs/CeO<sub>2</sub> NPs for protecting cells from oxidative damage. As shown in Figure 3B the viability of the cells incubated with 50 μM H<sub>2</sub>O<sub>2</sub> for 24 h was reduced to about 60%, whereas pretreatment with β-CDs/CeO<sub>2</sub> NPs (100 and 200 μg/mL) can prevent cellular damage triggered by H<sub>2</sub>O<sub>2</sub>. Furthermore, the intracellular ROS level was monitored using 2',7'-dichlorofluorescein diacetate as the fluorescence probe.<sup>46</sup> As shown in Figure 3C, a negligible fluorescence signal was observed when the cells were incubated with β-CDs/CeO<sub>2</sub> NPs compared with the control experiments. By contrast, high fluorescence signals were observed when the cells were incubated with H<sub>2</sub>O<sub>2</sub>. When the cells were pretreated with β-CDs/

CeO<sub>2</sub> NPs the fluorescence intensity of the H<sub>2</sub>O<sub>2</sub>-treated cells was significantly reduced, indicating the effective intracellular ROS scavenging activity of β-CDs/CeO<sub>2</sub> NPs. Oxidative stress plays a pivotal role in the pathogenesis of psoriasis.<sup>13</sup> Previous studies also found that antioxidants can improve the symptoms of psoriasis.<sup>10,14-19</sup> These results suggest that our system has a potential application in psoriasis therapy by suppressing ROS and protecting cells from oxidative stress.

### Anti-Psoriatic Efficacy in BALB/c Mice

Considering that the β-CDs on the CeO<sub>2</sub> NPs surface can be used as hydrophobic drug carriers, we loaded DIT, a classic psoriasis treatment drug, and investigated its anti-psoriatic efficacy in the IMQ-induced mouse model. For the convenience of administration, carbopol gel was chosen as the matrix of the DIT@β-CDs/CeO<sub>2</sub> NPs. After initiation of IMQ and DIT@β-CDs/CeO<sub>2</sub> NPs treatment, we calculated the PASI, performed H&E staining, and then calculated the weight ratio of spleen to body to evaluate the anti-psoriatic effect. The

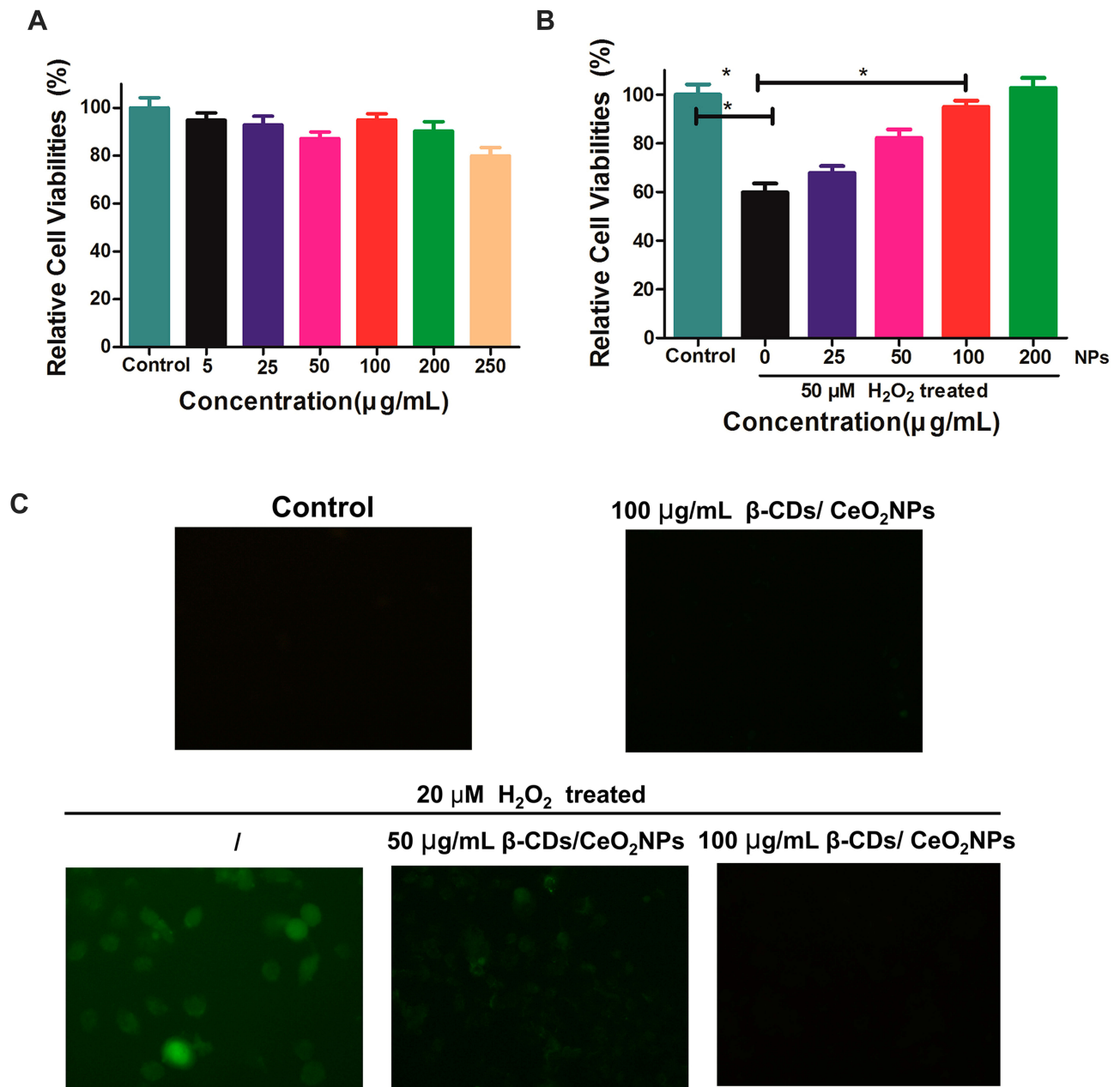


**Figure 3** (A) Viabilities of HaCaT incubated with varied concentrations of  $\beta$ -CDs/CeO<sub>2</sub> NPs for 48 h; (B) HaCaT viabilities for the protective capabilities of  $\beta$ -CDs/CeO<sub>2</sub> NPs by different doses after being treated with 50  $\mu$ M H<sub>2</sub>O<sub>2</sub>; (C) the fluorescence images of HaCaT cells after various treatments with H<sub>2</sub>O<sub>2</sub> (20  $\mu$ M) only,  $\beta$ -CDs/CeO<sub>2</sub> NPs (100  $\mu$ g/mL) only, H<sub>2</sub>O<sub>2</sub> and  $\beta$ -CDs/CeO<sub>2</sub> NPs stained with DCFH-DA.

erythema, scales, and thickness of PASI scored from 0 to 4 are shown in Figure 4A-D. The mice treated with DIT@ $\beta$ -CDs/CeO<sub>2</sub> NPs had lower mean scores for erythema, scales, and skin thickness than the mice treated with IMQ or DIT alone at the end of day 8. This result suggests that the DIT@ $\beta$ -CDs/CeO<sub>2</sub> NPs exerted a therapeutic effect on psoriasis and IMQ-induced skin inflammation.

The histopathology of the skin samples was performed to further confirm the anti-psoriatic effect of the DIT@ $\beta$ -

CDs/CeO<sub>2</sub> NPs. The phenotypic and the H&E-stained images of skin from different groups are shown in Figure 5. Severe erythema covered with white scales and marked inflammatory infiltration can be observed in the mice treated with IMQ compared with the normal mice. After treatment with different prescriptions, especially the IMQ+DIT@NPs group and IMQ+Halometasone (positive control) group, white scale and erythema of inflammatory skin were significantly reduced and consistent with the

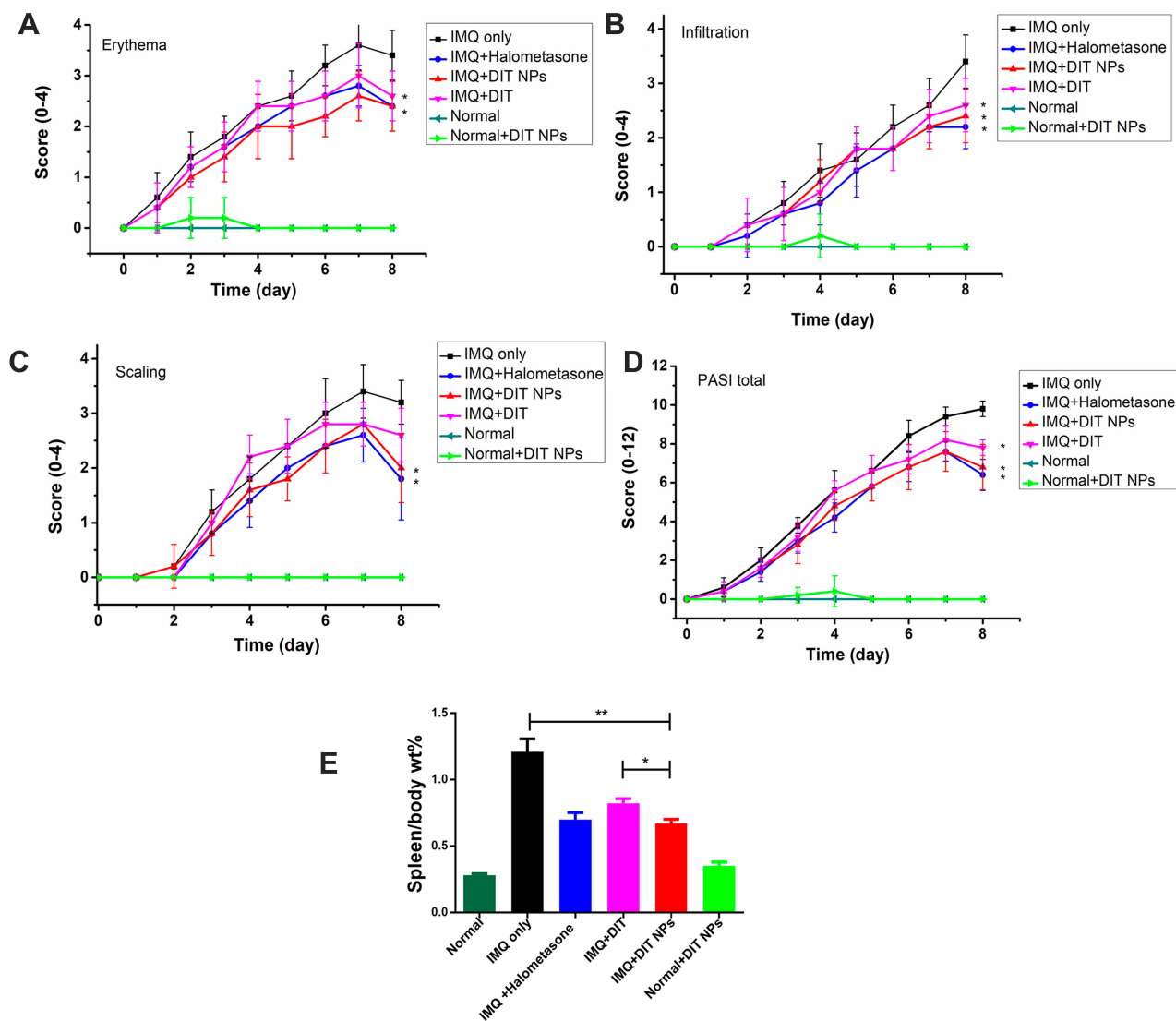


**Figure 4** Psoriasis Area and Severity Index (PASI) scoring of psoriatic dorsal regions of mice in different groups (n=5) were evaluated for 8 days, including erythema (A), scaling (B), infiltration of the mouse skin (C), with a scale from 0 to 4. The total score (D) was from 0 to 12.\*p < 0.05, compared with IMQ only group (n=5); The ratio of spleen weight to body weight (E) were recorded of IMQ and different treatment in different groups.

visual observation. These observations showed that the IMQ+ DIT@NPs were highly effective in alleviating the symptoms of IMQ-induced psoriasis in mice.

The spleen is the largest organ in the body's immune system, and the increased spleen/body wt% is an indicator reflecting the enhancement of immune activation-related diseases.<sup>43</sup> After 8 days of application with IMQ and different prescription, the mice were sacrificed and the weight ratio of spleen to body was calculated (Figure 4E). As expected, the weight ratio of spleen to body was the lowest in the normal mouse group and the highest in the IMQ-only group. Those of the IMQ+DIT@NPs group and IMQ+Halometasone (positive control) group were between the

normal mouse and IMQ-only groups. The calculated spleen/body weight% of the IMQ group ( $1.02 \pm 0.26$ ) was approximately three times larger than that of the normal mouse group ( $0.31 \pm 0.05$ ), and the results showed that the number of cells in the spleen significantly increased. The spleen/body weight % of the IMQ+DIT@NPs group was significantly lower than that of the IMQ-only group ( $p < 0.01$ ). In addition, the PASI score and spleen/weight % results indicated that the DIT@NPs was more effective than the DIT treatment. Overall, these results indicate that the dermal administration of the DIT@ $\beta$ -CDs/CeO<sub>2</sub> NPs effectively alleviated psoriasis, suggesting that the NPs may be used as a potential therapy for psoriasis.

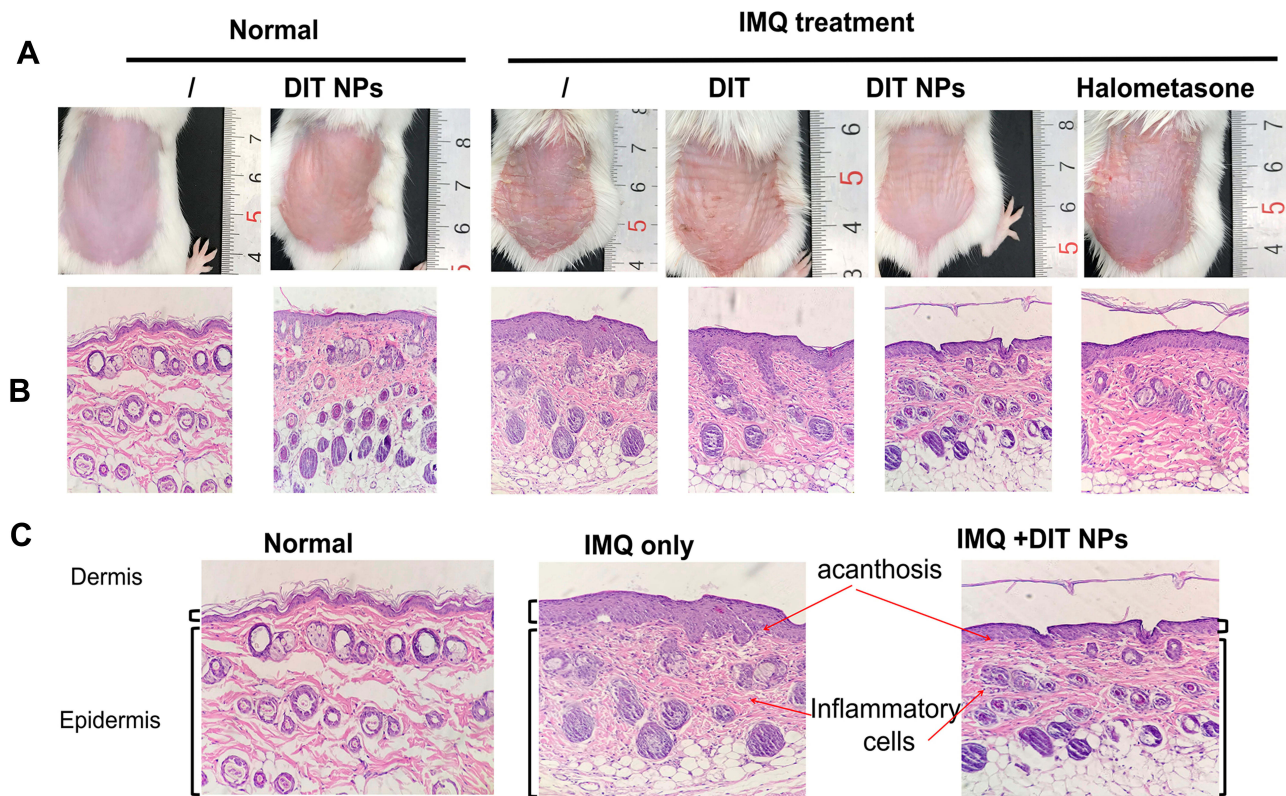


**Figure 5** Topical application of IMQ induced psoriatic like change on the dorsal skin of mice. At day 8, photographs were taken from the mice (A) and H&E staining (B) was performed to observe the differences of the treatment; (C) Enlarged view of normal mice group, the IMQ only group and IMQ+ DIT@β-CDs/CeO<sub>2</sub> NPs were also presented for annotation.

Psoriasis is a multifactorial disease with myriads of inflammatory mediators.<sup>1</sup> For instance, tumor necrosis factor (TNF)-α is overexpressed in psoriatic skins. We observed the effects of the NPs on the expression of TNF-α using immunofluorescence. As shown in Figure 6, TNF-α expression

obviously increased in the IMQ-treated mice compared with the control groups. However, the NPs significantly alleviated the TNF-α upregulation induced by IMQ. These findings suggest that the NPs display anti-psoriatic activities in vivo.

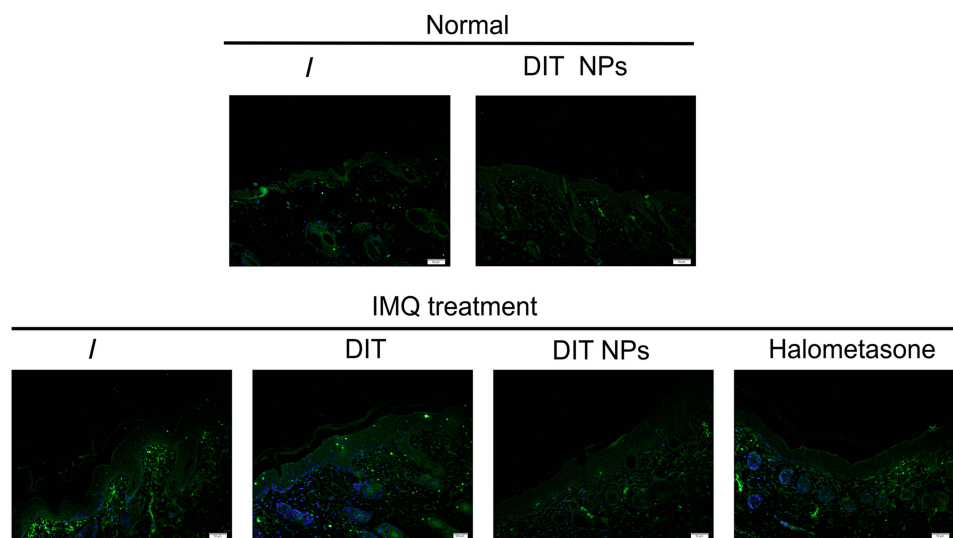


**Figure 6** The representative staining of TNF-α in psoriatic skins after different treatments including the healthy skin of normal mice, the diseased skin of psoriasis mice, the skin of psoriatic mice treated with DIT, DIT@NPs and Halometasone.

## Conclusion

In summary, we fabricated DIT@ $\beta$ -CDs/CeO<sub>2</sub> NPs exhibiting multi-enzyme mimic activity and functionally drug-loaded activities, which would rescue cells under oxidative stress and provide synergistic anti-psoriatic effects. The DIT could effectively be encapsulated in the inner cavity of  $\beta$ -CDs with a DL capacity of 3.48% and an EE of 94.7%. The  $\beta$ -CDs/CeO<sub>2</sub> NPs could effectively scavenge O<sub>2</sub><sup>•-</sup> and H<sub>2</sub>O<sub>2</sub> and provide remarkable cryoprotection against ROS-mediated damage. More importantly, the DIT@ $\beta$ -CDs/CeO<sub>2</sub> NPs provide an excellent therapeutic effect in IMQ-induced psoriatic model on the basis of morphological evaluation, PASI calculation, and inflammatory cytokine (TNF- $\alpha$ ) expression. This study paves the way toward the application of nanozyme  $\beta$ -CDs/CeO<sub>2</sub> NPs as a powerful tool for psoriasis therapy.

## Abbreviations

ROS, Reactive oxygen species;  $\beta$ -CD,  $\beta$ -cyclodextrin; NPs, nanoparticles; TEM, transmission electron microscopy; XPS, X-ray photoelectron spectroscopy; FT-IR, Fourier transform infrared spectrometry; SOD, superoxide dismutase; DIT, dithranol; IMQ, imiquimod; PASI, Psoriasis Area and Severity Index; PDI, polydispersity index (PDI); DL, drug loading; EE, entrapment efficiency; NBT, nitro-blue tetrazolium; MTT, 3-(4,5-dimethylthiazolyl)-2,5-diphenyltetrazolium bromide (MTT); TNF- $\alpha$ , tumor necrosis factor- $\alpha$ ; H&E, hematoxylin and eosin; SD, standard deviation.

## Acknowledgments

The authors are grateful for the generous financial support from the National Natural Science Foundation of China (No. 81973671, 21901186), the Natural Science Foundation of Shandong Province, China (ZR2019BB032), Project of Shandong Province Higher Educational Science and Technology Program (No. J18KA279).

## Disclosure

The authors report no conflicts of interest in this work.

## References

- Griffiths CEM, Barker JNWN. Pathogenesis and clinical features of psoriasis. *Lancet*. 2007;370(9583):263–271. doi:10.1016/S0140-6736(07)61128-3
- Papp KA, Reich K, Paul C, et al. A prospective Phase III, randomized, double-blind, placebo-controlled study of brodalumab in patients with moderate-to-severe plaque psoriasis. *Br J Dermatol*. 2016;175(2):273–286. doi:10.1111/bjd.14493
- Gelfand JM, Feldman SR, Stern RS, Thomas J, Rolstad T, Margolis DJ. Determinants of quality of life in patients with psoriasis: a study from the US population. *J Am Acad Dermatol*. 2004;51(5):704–708. doi:10.1016/j.jaad.2004.04.014
- Strober BE, van der Walt JM, Armstrong AW, et al. Clinical goals and barriers to effective psoriasis care. *Dermatol Ther*. 2019;9(1):5–18. doi:10.1007/s13555-018-0279-5
- Eberle F, Brück J, Holstein J, Hirahara K, Ghoreschi K. Recent advances in understanding psoriasis. *F1000Res*. 2016;5(770).
- Reindl J, Pesek J, Krüger T, et al. Proteomic biomarkers for psoriasis and psoriasis arthritis. *J Proteomics*. 2016;140:55–61. doi:10.1016/j.jprot.2016.03.040
- Seth D, Ehlert AN, Golden JB, et al. Interaction of resistin and systolic blood pressure in psoriasis severity. *J Invest Dermatol*. 2019;19:33401–33403.
- Conic RR, Damiani G, Schrom KP, et al. Psoriasis and psoriatic arthritis cardiovascular disease endotypes identified by red blood cell distribution width and mean platelet volume. *J Clin Med*. 2020;9(1):186. doi:10.3390/jcm9010186
- Lowes MA, Suárez-Fariñas M, Krueger JG. Immunology of Psoriasis. *Annu Rev Immunol*. 2014;32:227–255. doi:10.1146/annurev-immunol-032713-120225
- Utaş S, Köse K, Yazici C, Akdaş A, Keleştimur F. Antioxidant potential of propylthiouracil in patients with psoriasis. *Clin Biochem*. 2002;35(3):241–246. doi:10.1016/S0009-9120(02)00294-1
- Yildirim M, Inaloz H, Baysal V, Delibas N. The role of oxidants and antioxidants in psoriasis. *F1000Research*. 2003;17(1):34–36.
- Mittal M, Siddiqui MR, Tran K, Reddy SP, Malik AB. Reactive Oxygen Species in Inflammation and Tissue Injury. *Antioxid Redox Signal*. 2014;20(7):1126–1167. doi:10.1089/ars.2012.5149
- Zhou Q, Mrowietz U, Rostami-Yazdi M. Oxidative stress in the pathogenesis of psoriasis. *Free Radical Biol Med*. 2009;47(7):891–905. doi:10.1016/j.freeradbiomed.2009.06.033
- Lin X, Huang T. Oxidative stress in psoriasis and potential therapeutic use of antioxidants. *Free Radic Res*. 2016;50(6):585–595. doi:10.3109/10715762.2016.1162301
- Zhang S, Liu X, Mei L, Wang H, Fang F. Epigallocatechin-3-gallate (EGCG) inhibits imiquimod-induced psoriasis-like inflammation of BALB/c mice. *BMC Complement Altern Med*. 2016;16(1):334. doi:10.1186/s12906-016-1325-4
- Li P, Li Y, Jiang H, et al. Glabridin, an isoflavan from licorice root, ameliorates imiquimod-induced psoriasis-like inflammation of BALB/c mice. *Int Immunopharmacol*. 2018;59:243–251. doi:10.1016/j.intimp.2018.04.018
- Lai R, Xian D, Xiong X, Yang L, Song J, Zhong J. Proanthocyanidins: novel treatment for psoriasis that reduces oxidative stress and modulates Th17 and Treg cells. *Redox Rep*. 2018;23(1):130–135. doi:10.1080/13510002.2018.1462027
- Simpson BS, Luo X, Costabile M, et al. Polyandric acid A, a Clerodane diterpenoid from the Australian medicinal plant *Dodonaea polyandra*, attenuates pro-inflammatory cytokine secretion in vitro and in vivo. *J Nat Prod*. 2014;77(1):85–91. doi:10.1021/np400704b
- Yang G, Li S, Yang Y, et al. Nobiletin and 5-hydroxy-6,7,8,3',4'-pentamethoxyflavone ameliorate 12-O-tetradecanoylphorbol-13-acetate-induced psoriasis-like mouse skin lesions by regulating the expression of Ki-67 and proliferating cell nuclear antigen and the differentiation of CD4<sup>+</sup> T cells through mitogen-activated protein kinase signaling pathways. *J Agric Food Chem*. 2018;66(31):8299–8306. doi:10.1021/acs.jafc.8b02524
- Chen S, Han K, Li H, et al. Isogarcinol extracted from *Garcinia mangostana* L. Ameliorates imiquimod-induced psoriasis-like skin lesions in mice. *J Agric Food Chem*. 2017;65(4):846–857. doi:10.1021/acs.jafc.6b05207
- Wei H, Wang E. Nanomaterials with enzyme-like characteristics (nanozymes): next-generation artificial enzymes. *Chem Soc Rev*. 2013;42(14):6060–6093. doi:10.1039/c3cs35486e

22. Huang Y, Ren J, Qu X. Nanozymes: classification, catalytic mechanisms, activity regulation, and applications. *Chem Rev.* 2019;119(6):4357–4412. doi:10.1021/acs.chemrev.8b00672
23. Singh N, Savanur MA, Srivastava S, D'Silva P, Muges G. A redox modulatory Mn<sub>3</sub>O<sub>4</sub> nanozyme with multi-enzyme activity provides efficient cytoprotection to human cells in a parkinson's disease model. *Angew Chem Int Ed.* 2017;56(45):14267–14271. doi:10.102/anie.201708573
24. Kwon HJ, Cha M-Y, Kim D, et al. Mitochondria-targeting ceria nanoparticles as antioxidants for alzheimer's disease. *ACS Nano.* 2016;10(2):2860–2870. doi:10.1021/acsnano.5b08045
25. Yang X, Yang Y, Gao F, Wei -J-J, Qian C-G, Sun M-J. Biomimetic hybrid nanozymes with self-supplied H<sup>+</sup> and accelerated O<sub>2</sub> generation for enhanced starvation and photodynamic therapy against hypoxic tumors. *Nano Lett.* 2019;19(7):4334–4342. doi:10.1021/acs.nanolett.9b00934
26. Fan L, Xu X, Zhu C, et al. Tumor catalytic–photothermal therapy with yolk–shell gold@carbon nanozymes. *ACS Appl Mater Interfaces.* 2018;10(5):4502–4511. doi:10.1021/acsmi.7b17916
27. Liu C, Xing J, Akakuru OU, et al. Nanozymes-engineered metal–organic frameworks for catalytic cascades-enhanced synergistic cancer therapy. *Nano Lett.* 2019;19(8):5674–5682. doi:10.1021/acs.nanolett.9b02253
28. Rajkovic O, Gourmel C, d'Arcy R, et al. Reactive oxygen species-responsive nanoparticles for the treatment of ischemic stroke. *Adv Ther.* 2019;2(7):1900038. doi:10.1002/adtp.201900038
29. Zhang K, Tu M, Gao W, et al. Hollow prussian blue nanozymes drive neuroprotection against ischemic stroke via attenuating oxidative stress, counteracting inflammation, and suppressing cell apoptosis. *Nano Lett.* 2019;19(5):2812–2823. doi:10.1021/acs.nanolett.8b04729
30. Ni D, Wei H, Chen W, et al. Ceria nanoparticles meet hepatic ischemia-reperfusion injury: the perfect imperfection. *Adv Mater.* 2019;31(40):1902956. doi:10.1002/adma.201902956
31. Wang G, Zhang J, He X, Zhang Z, Zhao Y. Ceria nanoparticles as enzyme mimetics. *Chin J Chem.* 2017;35(6):791–800. doi:10.1002/cjoc.201600845
32. Nicolini V, Gambuzzi E, Malavasi G, et al. Evidence of catalase mimetic activity in Ce<sup>3+</sup>/Ce<sup>4+</sup> doped bioactive glasses. *J Phys Chem B.* 2015;119(10):4009–4019. doi:10.1021/jp511737b
33. Kim CK, Kim T, Choi I-Y, et al. Ceria nanoparticles that can protect against ischemic stroke. *Angew Chem Int Ed.* 2012;51(44):11039–11043. doi:10.1002/anie.201203780
34. Kim J, Kim HY, Song SY, et al. Synergistic oxygen generation and reactive oxygen species scavenging by manganese ferrite/ceria co-decorated nanoparticles for rheumatoid arthritis treatment. *ACS Nano.* 2019;13(3):3206–3217. doi:10.1021/acsnano.8b08785
35. Heckman KL, DeCoteau W, Estevez A, et al. Custom cerium oxide nanoparticles protect against a free radical mediated autoimmune degenerative disease in the brain. *ACS Nano.* 2013;7(12):10582–10596. doi:10.1021/nn403743b
36. Damiani G, Pacifico A, Linder DM, et al. Nanodermatology-based solutions for psoriasis: state-of-the art and future prospects. *Dermatol Ther.* 2019;32(6):e13113. doi:10.1111/dth.13113
37. DeLouise LA. Applications of Nanotechnology in Dermatology. *J Invest Dermatol.* 2012;132(3):964–975. doi:10.1038/jid.2011.425
38. Crini G. Review: a history of Cyclodextrins. *Chem Rev.* 2014;114(21):10940–10975. doi:10.1021/cr500081p
39. Liu K, Jiang X, Hunziker P. Carbohydrate-based amphiphilic nano delivery systems for cancer therapy. *Nanoscale.* 2016;8(36):16091–16156.
40. Sun T, Wang Q, Bi Y, et al. Supramolecular amphiphiles based on cyclodextrin and hydrophobic drugs. *J Mater Chem B.* 2017;5(14):2644–2654. doi:10.1039/C6TB03272A
41. Bonnet V, Gervaise C, Djedaïni-Pilard F, Furlan A, Sarazin C. Cyclodextrin nanoassemblies: a promising tool for drug delivery. *Drug Discov Today.* 2015;20(9):1120–1126. doi:10.1016/j.drudis.2015.05.008
42. Yu N, Hao J, Wang Q, Huang K, Geng B. Self-assembled porous ceria nanostructures with excellent water solubility and antioxidant properties. *RSC Adv.* 2016;6(51):45957–45962. doi:10.1039/C6RA05630J
43. Sun L, Liu Z, Wang L, et al. Enhanced topical penetration, system exposure and anti-psoriasis activity of two particle-sized, curcumin-loaded PLGA nanoparticles in hydrogel. *J Controlled Release.* 2017;254:44–54. doi:10.1016/j.jconrel.2017.03.385
44. Ali SS, Hardt JI, Quick KL, et al. A biologically effective fullerene (C60) derivative with superoxide dismutase mimetic properties. *Free Radical Biol Med.* 2004;37(8):1191–1202. doi:10.1016/j.freeradbiomed.2004.07.002
45. Pirmohamed T, Dowding JM, Singh S, et al. Nanoceria exhibit redox state-dependent catalase mimetic activity. *Chem Commun.* 2010;46(16):2736–2738. doi:10.1039/b922024k
46. Li X-J, Li W-T, Li Z-H-R, et al. Iron-chelated polydopamine decorated doxorubicin-loaded nanodevices for reactive oxygen species enhanced cancer combination therapy. *Front Pharmacol.* 2019;10:75.
47. Kang N-W, Kim M-H, Sohn S-Y, et al. Curcumin-loaded lipid-hybridized cellulose nanofiber film ameliorates imiquimod-induced psoriasis-like dermatitis in mice. *Biomaterials.* 2018;182:245–258. doi:10.1016/j.biomaterials.2018.08.030
48. Montini T, Melchionna M, Monai M, Fornasiero P. Fundamentals and catalytic applications of CeO<sub>2</sub>-based materials. *Chem Rev.* 2016;116(10):5987–6041. doi:10.1021/acs.chemrev.5b00603
49. Xu C, Lin Y, Wang J, et al. Nanoceria-triggered synergetic drug release based on CeO<sub>2</sub>-capped mesoporous silica host–guest interactions and switchable enzymatic activity and cellular effects of CeO<sub>2</sub>. *Adv Healthc Mater.* 2013;2(12):1591–1599. doi:10.1002/adhm.201200464
50. Chen X, Parker SG, Zou G, Su W, Zhang Q. β-Cyclodextrin-functionalized silver nanoparticles for the naked eye detection of aromatic isomers. *ACS Nano.* 2010;4(11):6387–6394. doi:10.1021/nn1016605
51. Song S, Chong Y, Fu H, Ning X, Shen H, Zhang Z. HP-β-CD functionalized Fe<sub>3</sub>O<sub>4</sub>/CNPs-based theranostic nanopatform for ph/nir responsive drug release and mr/nirfl imaging-guided synergetic chemo/photothermal therapy of tumor. *ACS Appl Mater Interfaces.* 2018;10(40):33867–33878. doi:10.1021/acsmi.8b09999
52. Yang B, Chen Y, Shi J. Reactive Oxygen Species (ROS)-Based Nanomedicine. *Chem Rev.* 2019;119(8):4881–4985. doi:10.1021/acs.chemrev.8b00626

## International Journal of Nanomedicine

### Publish your work in this journal

The International Journal of Nanomedicine is an international, peer-reviewed journal focusing on the application of nanotechnology in diagnostics, therapeutics, and drug delivery systems throughout the biomedical field. This journal is indexed on PubMed Central, MedLine, CAS, SciSearch®, Current Contents®/Clinical Medicine,

Submit your manuscript here: <https://www.dovepress.com/international-journal-of-nanomedicine-journal>

Dovepress

Journal Citation Reports/Science Edition, EMBase, Scopus and the Elsevier Bibliographic databases. The manuscript management system is completely online and includes a very quick and fair peer-review system, which is all easy to use. Visit <http://www.dovepress.com/testimonials.php> to read real quotes from published authors.